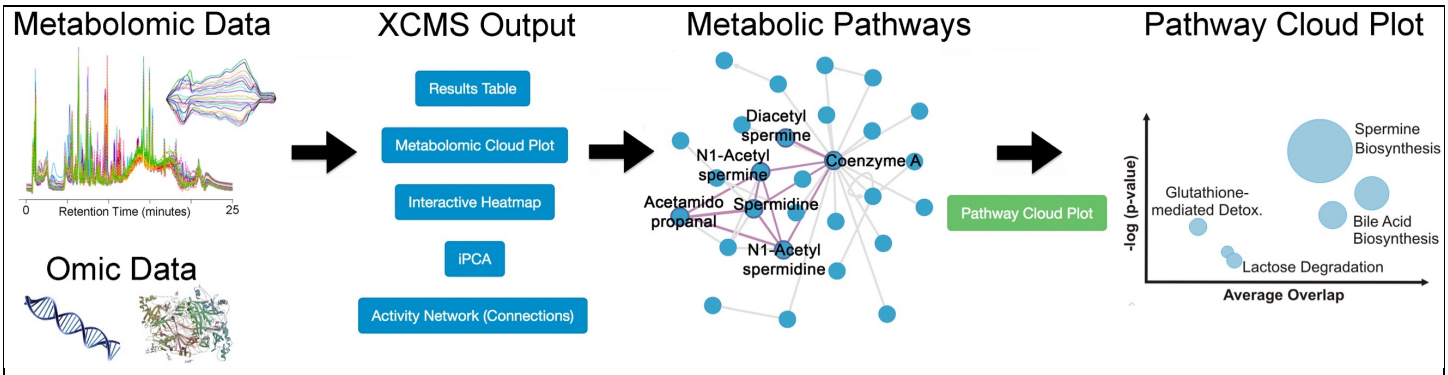

Supplementary Figure 1

Overview of the systems biology platform.

Raw LC-MS data is processed in XCMS Online. The XCMS output is directly used to identify dysregulated metabolic pathways with predictive pathway enrichment algorithm. Protein and gene data is then integrated to perform the systems-level analysis and generate the pathway cloud plot and systems biology results table (not shown in the figure).

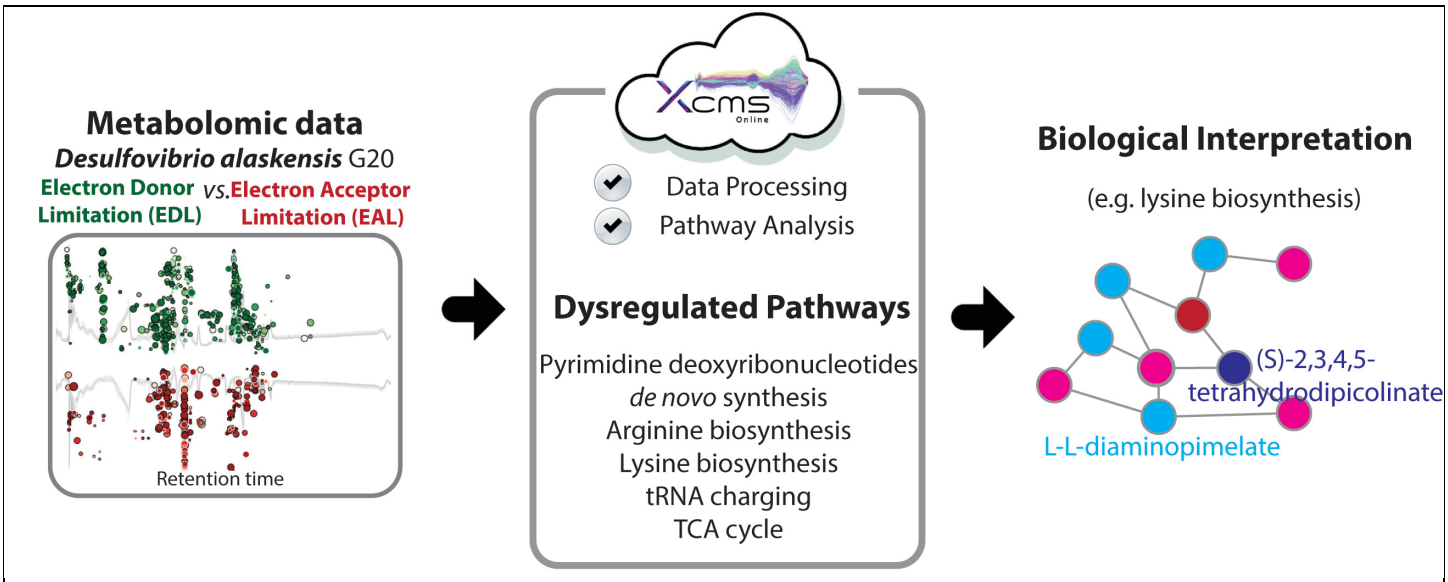

Supplementary Figure 2

Example of predictive pathway analysis

Schematic display of predictive pathway analysis on G20 metabolomic data to decipher biological roles during the process of metal corrosion.

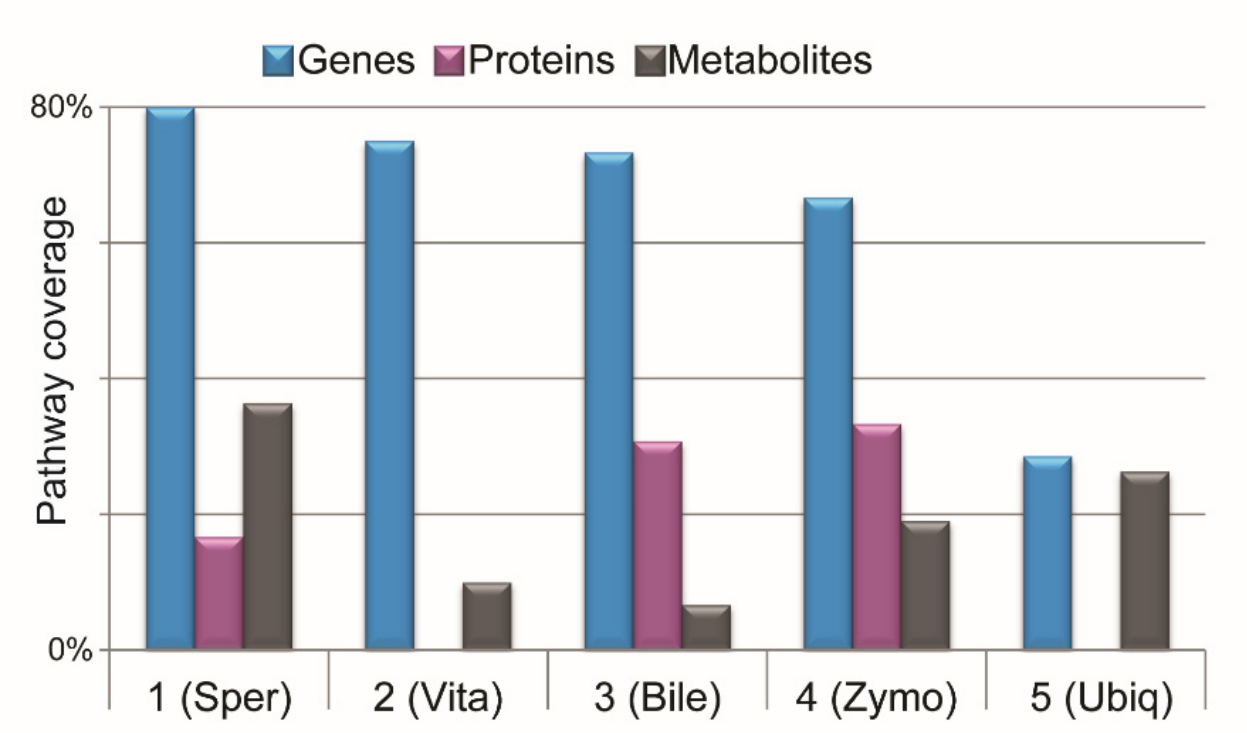

Supplementary Figure 3

Percent pathway coverage using multi-omic analysis of colon cancer data.

The bar graph presents gene, protein and metabolite overlap on dysregulated metabolic pathways identified using predictive pathway analysis. These pathways also have a previously known association with colon cancer.

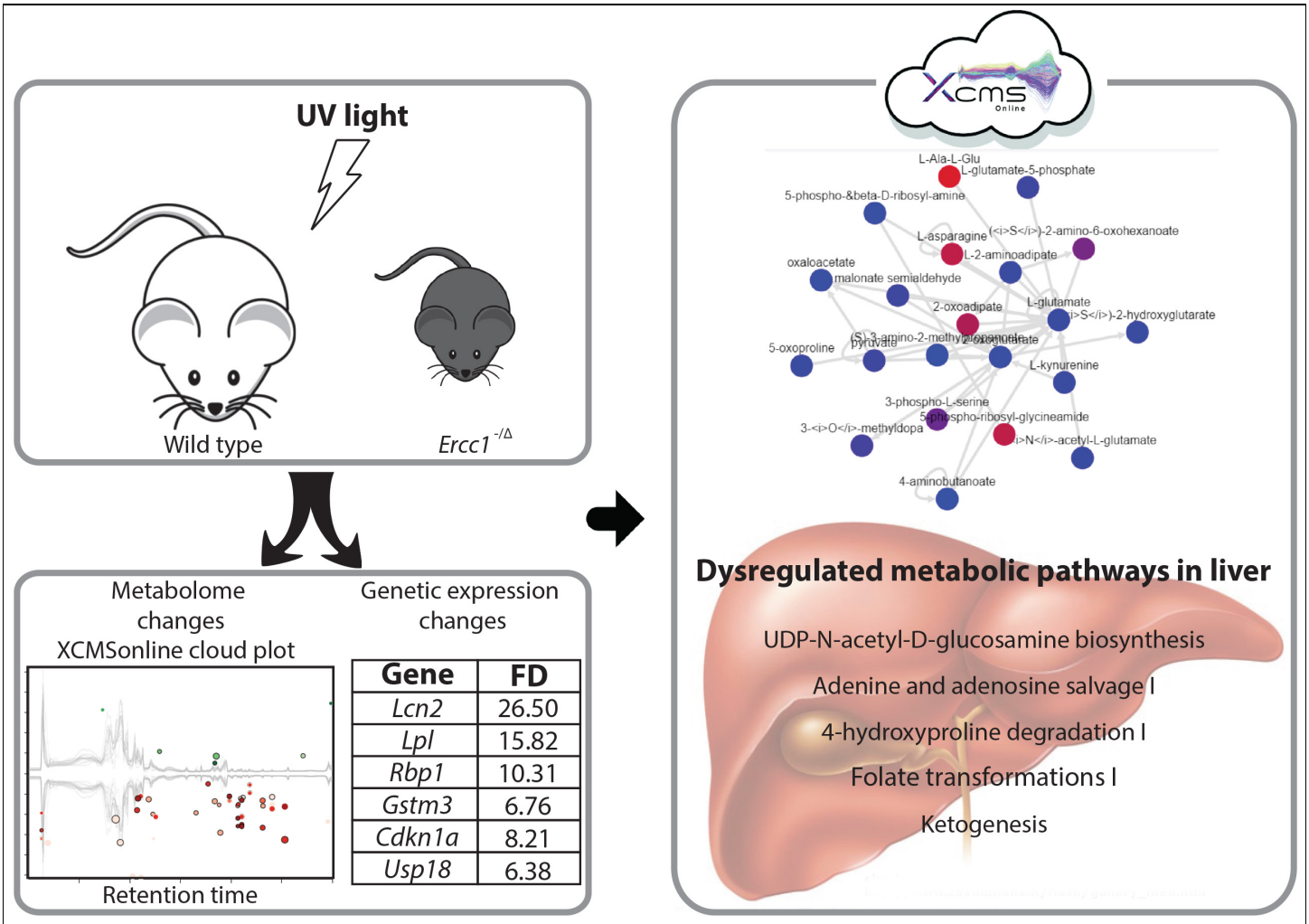

Supplementary Figure 4

Integrated metabolomics and transcriptomics data analysis.

Schematic of multi-omic analysis of *Ercc1*$^{-/\Delta}$ mouse model using the XCMS Online systems biology platform in a study of XFE progeroid syndrome showing overlapping dysregulated pathways.

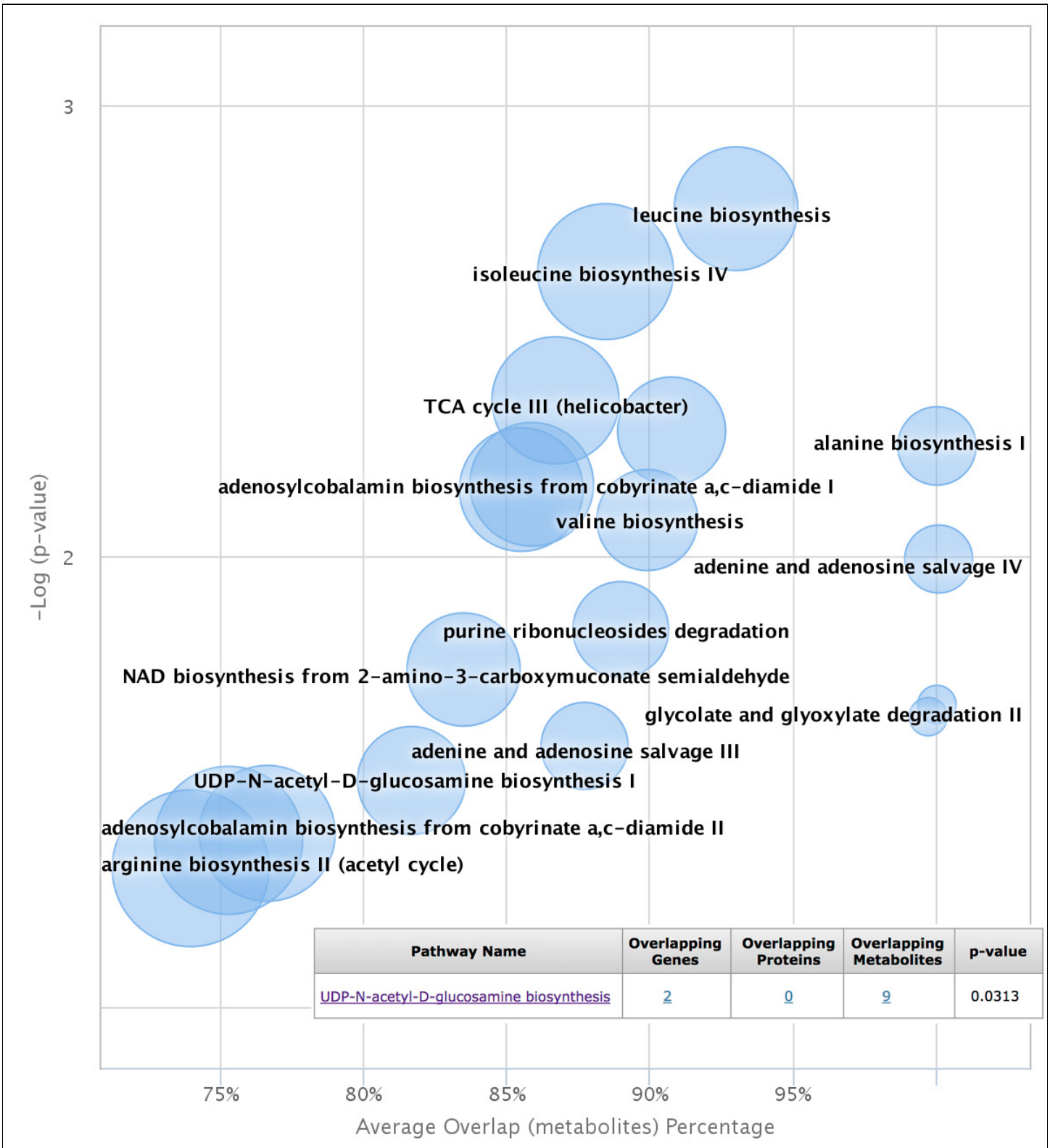

Pathway Name	Overlapping Genes	Overlapping Proteins	Overlapping Metabolites	p-value
UDP-N-acetyl-D-glucosamine biosynthesis	2	0	9	0.0313

Supplementary Figure 5

Pathway cloud plot for DvH nitrate stress with integrated omics.

Plot focuses on *p*-value < 0.05 illustrating 18 dysregulated pathways and three overlapping genes *leuA* (leucine biosynthesis), *glmU* and *glmS* (UDP-N-acetyl-D-glucosamine biosynthesis). Pathways are plotted as a function of FET pathway significance versus average metabolic pathway overlap, with the radius of the circle representing the size of the metabolic pathway. Significantly dysregulated pathways appear in the upper right-hand quadrant of the plot. Each circle presents overlapping gene, protein and metabolite data when cursor is hovered over, as demonstrated for UDP-N-acetyl-D-glucosamine biosynthesis pathway. Clicking on these table features gives additional specific pathway, gene, protein and metabolite information.

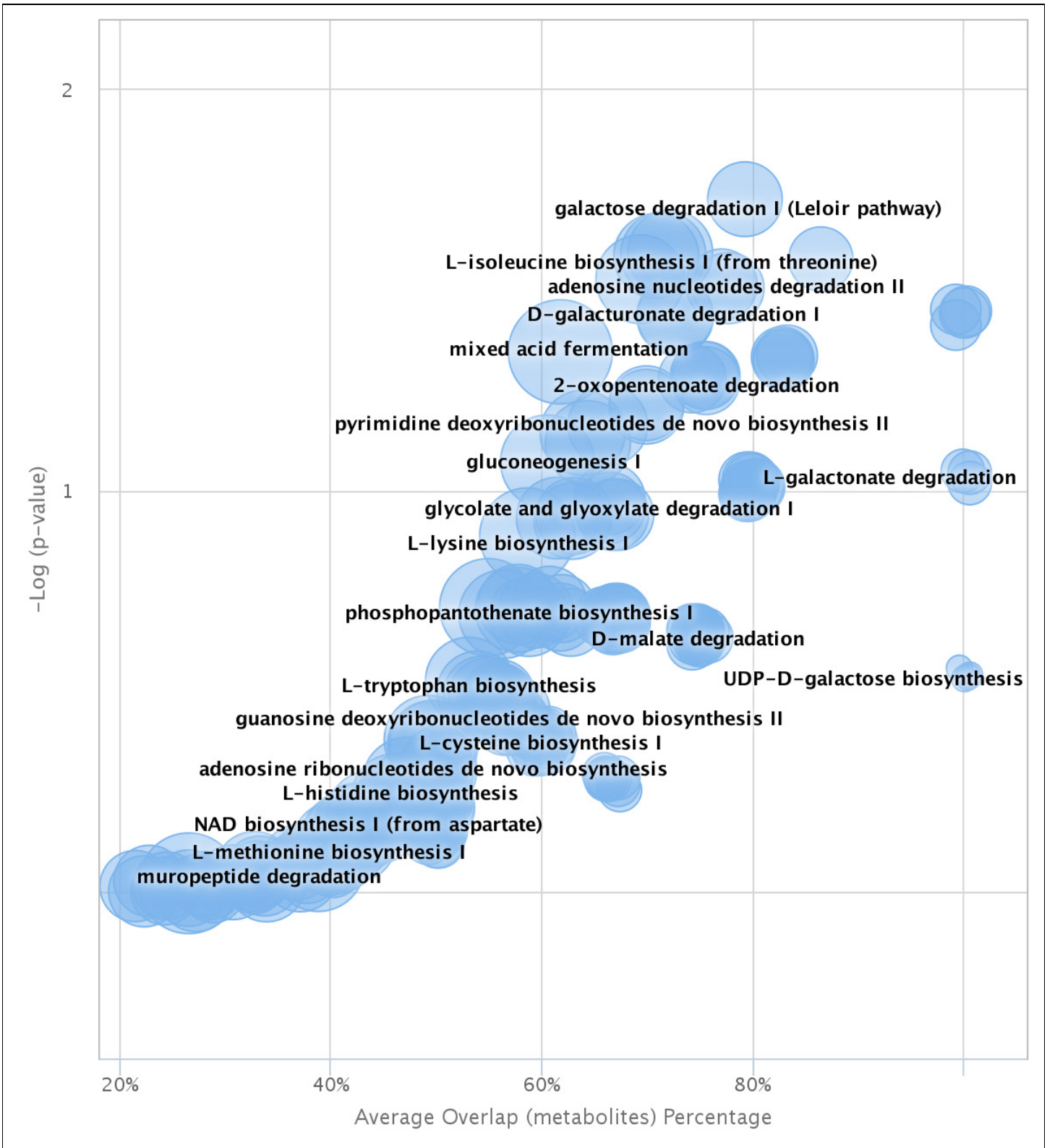

Supplementary Figure 6

Pathway cloud plot presenting all dysregulated metabolic pathways under the effects of different carbon sources.

Here a total overview of the pathway cloud plot is presented to illustrate the all the identified pathways ranging from 0.0055 < *p*-value < 1. Significance of the pathway overlap (-log(p-value)) versus the percent overlap of the metabolites found in each pathway shows dysregulated features of greater interest in the upper right-hand quadrant of the plot. The radius of the circles represents the overall size of the metabolic pathway.

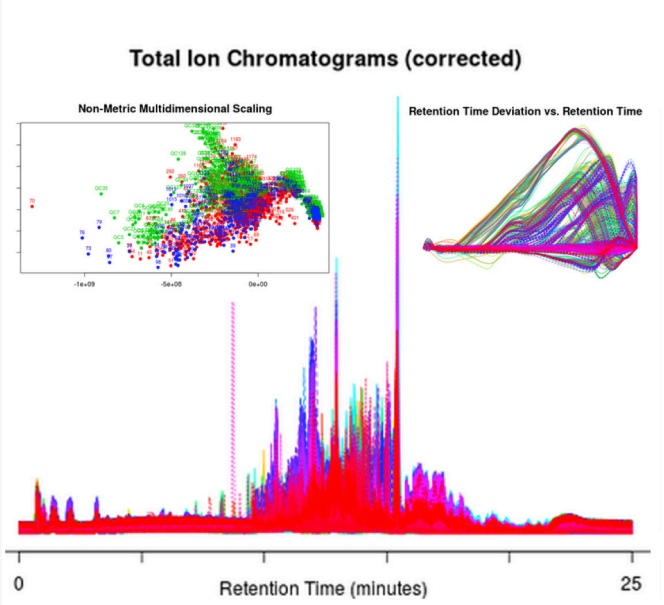

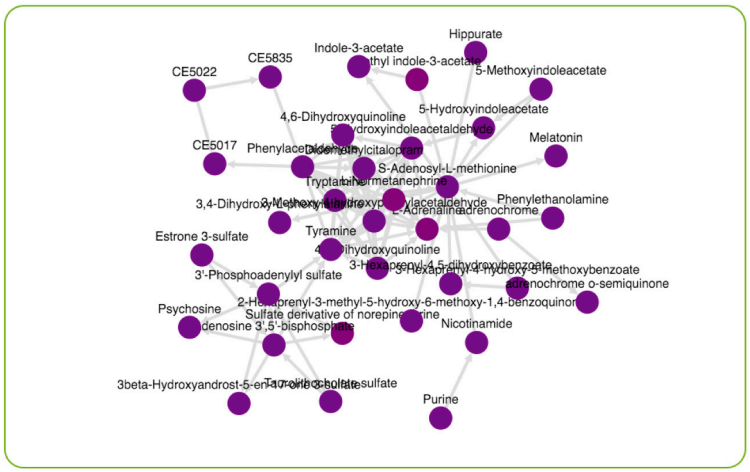

Top pathways

Download as CSV

Pathways	overlap_size	pathway_size	p-value (raw)	p-value
Omega-6 fatty acid metabolism	9	10	0.00082	0.00093
Mono-unsaturated fatty acid beta-oxidation	8	9	0.00203	0.00099

Supplementary Figure 7

Scalability of XCMS analysis with large sample cohort.

Predictive pathway analysis generated from metabolomic data on the 1,600 human samples, two top pathways shown.

Supplementary Methods

XCMS Systems Biology Platform Development and Multi-Omic Workflow

The metabolomics guided multi-omic workflow (**Supplementary Figure 1**) builds upon XCMS analysis of metabolomics data to identify connections between metabolites, dysregulated pathways and overlapping genes and proteins involved in those pathways. Multi-omic analysis can be performed in pairwise, multi-group and meta XCMS jobs. Data files are uploaded into individual sample class datasets in order to perform retention time correction, peak alignment, feature selection and univariate statistical analysis based on user defined *p*-value (default = 0.01), generating a results table of significantly dysregulated features, which is then used to metabolic network and pathway analysis followed by multi-omic analysis with uploaded gene and/or protein data. Detailed video instructions are provided on how to use XCMS systems biology platform, including pathway analysis and integrated omics (https://xcmsonline.scripps.edu/landing_page.php?pgcontent=institute) as well as Pathway Cloud Plot (https://xcmsonline.scripps.edu/landing_page.php?pgcontent=institute). Complete documentation and instructions on how to use XCMS Online are provided (https://xcmsonline.scripps.edu/landing_page.php?pgcontent=documentation). The code for all the mentioned algorithms and computer programs are currently not available.

Metabolite Pathway Analysis

The *mummichog* algorithm[1] has been improved for use with XCMS including additional visualizations of the network results. In brief, the algorithm takes the accurate mass of significant metabolites from the results table and uses a Fisher's exact test (FET) to assess the significance of the pathways with *p*-values, which can be specified for any of the >7600 metabolic models available on XCMS. Meanwhile, a list of permutation features (equal length to the significant metabolite list) is generated by randomly sampling of the results table and used to calculate the *p*-values for all the pathways. This step is repeated to calculate a cumulative distribution function, which is used to adjust the *p*-value per pathway calculated from the significant list.

Integrated Omics

Following the prediction of enriched metabolic pathways, the user uploads a list of significant genes and/or proteins from transcriptomic and proteomic data to perform multi-scale omics analysis. Differentially expressed gene and protein data should be in the form of a comma separated (.csv) or tab separated (.tsv) file and data format should be in gene name (gene or protein data) and UniProt accession ID (protein data). The integrated omics analysis on XCMS Online then performs gene/protein matching onto the previously predicted pathways. A matching algorithm was developed in our lab to perform the

Nature Methods doi:10.1038/nmeth.4260

analysis. Gene and protein data are uploaded in tab separated value format using gene symbol accession IDs for genes and either gene symbol or Uniprot accession IDs for proteins. The user defines the type of list and runs the matching sub-job. The matching algorithm reads the user input data and known pathway associated data in the format of strings and considers it a match if the strings are identical. The matched genes and/or proteins are displayed and compared with the total number of associated genes and/or proteins to obtain pathway overlap. Once the integrated omics job is completed, the result will be presented in a table, showing both the overlapped and total number of gene/protein/metabolite for each pathway. A web link is provided for each overlap/total number to list the detailed genes/proteins/metabolites. Further, clicking each listed gene/protein/metabolite links to database sources for more information (gene information from BioCyc, protein information from UniProt, and metabolite information from KEGG and METLIN). Each pathway also has a web link connected to BioCyc that allows the user to view more detailed information about the pathway.

Pathway Cloud Plot

Once the pathway prediction and/or multi-omic overlap analysis is completed, a multi-omic cloud plot is generated to provide simple visualization of all the dysregulated metabolic pathways in a single plot. Statistical significance of the pathway match is plotted versus the percent pathway overlap; the trend towards significant pathways with more coverage are in the upper right-hand quadrant and the radius of the bubble represents the size of pathway in terms of its metabolites. The bubble size can be adjusted to present the best plot view by tuning the bar on the top right side of the plot. Clicking the bubble allows the user to see a table of the overlapped genes, proteins and metabolites, linking to database sources for more information. The user can also adjust the *p*-value threshold on the top left side of the plot to refine and display only certain pathways with their *p*-values smaller than the threshold.

Databases Queried

Species-specific pathway information was archived from BioCyc (version 19.5 – 20.0) together with their associated genes, proteins, and metabolites. For pathway analysis, the metabolite information queries BioCyc. For multi-omic integration, Uniprot is archived to get the correlations between Uniprot protein accession IDs and BioCyc protein accession IDs so that the user can upload protein data with either Uniprot or BioCyc formats. In the display of pathway/multi-omic analysis, detailed gene/protein information is from BioCyc and metabolite information is from both KEGG and METLIN. Currently, over 7600 metabolic species are provided in the platform (https://xcmsonline.scripps.edu/pathway/biosources.php). These pathway databases are organized into tiers according to the amount of manual review and updating they have received. Among them, Tier 1 (http://biocyc.org/biocyc-pgdb-list.shtml#tier1) databases have been created through intensive manual efforts and received at least a year of literature-based curation. In comparison, Tier 2 and Tier 3

databases (http://biocyc.org/biocyc-pgdb-list.shtml#tier2) contain computational predicted metabolic pathways and underwent less than one year of literature-based curation (typically 1-4 months). Data are stored in a relational database management system and accessed with structured query language (SQL). The user interface of the analytical platform was programmed in PHP, HTML5, and JavaScript. Once the user uploads transcriptomic and/or proteomic data, sub jobs are created to search against the same identified pathways to tabulate the overlapping genes and proteins by pathway. The background processing can be monitored by the users with log files available to confirm the job has processed correctly. Distinct genes and proteins are counted after removing duplicates and are displayed on the pathway summary table. Total genes and proteins are counted provided they occur at least once in the pathway of interest.

Supplementary Note

Below we describe seven examples of the new XCMS Online workflow for performing systems biology using predictive pathway analysis and integrated omics. All examples include predictive pathway analysis, which is now performed automatically after XCMS metabolomic data processing for retention time alignment, peak picking and statistical analysis. Additional examples are presented with transcriptomic and proteomic data integration. As XCMS Online continues to grow, so does the demand for processing power. To illustrate the scalability of this workflow, we also present an example on a large dataset containing a 1600 samples.

S1. Progenitor Cell Proliferation Study

Multiple sclerosis is a demyelinating disease in which the insulating covers of nerve cells in the brain and spinal cord are progressively damaged. Previous studies have revealed that the primary mechanism of multiple sclerosis involves the failure of the precursor oligodendrocyte cells (OPCs) to proliferate and differentiate, which further leads to the defect of its remyelination[2]. In this study, OPC differentiation is investigated on a metabolomics level to understand its molecular mechanisms, which potentially allows to identify active small molecules to promote the myelination of the OPCs.

Cell culture and global metabolomics.

Rat primary optic nerve OPCs were isolated by panning (>99% $A2B5^+$) and cultured in poly-D-lysine (10 $mg \cdot mL^{-1}$) coated tissue culture dishes in OPC culture media (Neurobasal Media, Invitrogen) supplemented with B27-without vitamin A (Invitrogen), non-essential amino acids, L-glutamine, penicillin/streptomycin, β-mercaptoethanol and PDGF-AA (50 $ng \cdot mL^{-1}$; Peprotech)) at 37°C with 5% CO_2. The culture medium was replaced every 48h and cells were collected before the confluency reached 60% to maintain a naive state. For differentiation, OPCs with 1.7×10^5 cells/well were plated in differentiation media (Neurobasal Media (Invitrogen) supplemented with B27-without vitamin A (Invitrogen), non-essential amino acids, L-glutamine and PDGF-AA (2 $ng \cdot mL^{-1}$; Peprotech)). Triiodothyronine (T3) and DMSO were used as the positive and negative controls, respectively. Cells were collected at different times for *in vitro* myelination and metabolomics studies.

Cells incubated in the differentiation medium were collected at day 6 for both the T3 and DMSO treated OPC. The cells were rinsed twice with PBS to completely remove the culture medium and then scraped into a 1.5 mL Eppendorf vial using 500–1000 μL PBS. Subsequently, the cells were collected by aspirating the supernatant after centrifugation at 12,000 rpm at 4°C for 15 min. The metabolites were extracted from cell pellets by a methanol:acetonitrile:water (2:2:1, v/v) solvent mixture. A volume of 600 μL of cold solvent was added to each pellet, vortexed for 30 s, and soaked in liquid nitrogen for 1

min. The samples were then allowed to thaw at room temperature and then sonicated for 10 min. This freeze-thaw process was repeated for additional 2X. To further precipitate proteins, the samples were incubated for 1 h at −20°C, followed by centrifugation at 16,000 × g and 4°C for 15 min. The protein concentrations of the cell pellets were measured after centrifugation using a bicinchoninic acid assay (BCA assay). The resulting supernatant was removed and evaporated to dryness in a vacuum concentrator (LABCONCO CentriVap Benchtop). The dry extracts were then reconstituted in the appropriate volume of acetonitrile/water (1:1, v/v), normalized by the protein concentration with the lowest concentration approximately 50 μL, sonicated for 10 min, and centrifuged for 15 min at 16,000 × g and 4°C to remove insoluble debris. The supernatants were transferred to HPLC vials with inserts and stored at −80°C prior to LC-MS analysis.

Cell extracts were analyzed on a 6550 iFunnel QTOF mass spectrometer (Agilent Technologies) coupled with a 1290 UPLC system (Agilent Technologies). HPLC was carried out on a Luna NH_2, 3 μm, 150 mm × 1.0 mm I.D. HILIC column (Phenomenex). The mobile phase was composed of A = 20 mM ammonium acetate and 40 mM ammonium hydroxide in 95% water (v/v) and B = 95% acetonitrile. The remaining 5% components were either acetonitrile or water, respectively. A linear gradient from 100% B (0–5 min) to 100% A (50–55 min) was applied. A 10 min re-equilibration time was applied to the HILIC column for re-equilibration and maintenance of reproducibility. The flow rate was 50 μL/min, and the sample injection volume was 5 μL. Electrospray ionization source conditions were set as follows: dry gas temperature, 200 °C; flow, 11 L/min, fragmentor, 380 V; sheath gas temperature, 300 °C; flow, 9 L/min; nozzle voltage, 500 V; capillary voltage, −500 V in ESI negative mode. The instrument was set to acquire data over the m/z range 50–1000, with the MS acquisition rate of 1 spectra/s. The sample sequence was randomized to avoid systematic decreases in signals over sample sets. For the MS/MS of selected precursors, the default isolation width was set as narrow (~1.3 m/z), with MS acquisition rate set at 2 spectra/s and MS/MS acquisition at 2 spectra/s to acquire over the m/z range 50–1000 and 25–1000; respectively. MS/MS data were acquired at the collision energy of 20 V.

LC-MS data were converted to mzXML files using MassHunter Acquisition Software (Agilent MassHunter 6.0B). The mzXML files were uploaded to XCMS Online for data processing including peak detection, retention time correction, profile alignment, and isotope annotation. Data were processed using both pairwise and multigroup comparison and the parameter settings were as follows: centWave for feature detection (Δ m/z = 15 ppm, minimum peak width = 10 s, and maximum peak width = 60 s); obiwarp settings for retention time correction (profStep = 0.5); parameters for chromatogram alignment, including mzwid = 0.015, minfrac = 0.5, and bw = 5. The relative quantification of metabolite features was based on extracted ion chromatogram (EIC) areas. Paired parametric two-way t-test and one-way ANOVA (post hoc Tukey test) were used to test the variation pattern of metabolite features between and

across cell samples collected at different times after being treated with T3 and DMSO. Multigroup analysis and pairwise comparisons between DMSO and T3 at individual incubation times were conducted. The results output, including EICs, pairwise/multigroup cloud plot, multidimensional scaling plots, and principle components were exported directly from XCMS Online. Generally, the numbers of total pairwise dysregulated features and significantly altered features (statistically defined as $p < 0.01$, including both upregulated and downregulated features) were reported in this study.

Pathway analysis results.

Bypassing the time-consuming metabolite identification prior to metabolic pathway analysis, our systems biology platform allowed for the rapid identification of dysregulated metabolic pathways, providing instant and useful guidance for further analytical and biological experiments. In this particular case, we observed the significant changes of several metabolic pathways in the process of OPCs differentiation induced by T3. These pathways include glutamate metabolism, glutathione metabolism and tryptophan metabolism. To the best of our knowledge, there are very few literature reports on the metabolomic profiling of OPCs during cell differentiation. However, it is worth noting that those pathway-related metabolites are also found in several metabolomic studies on the pluripotent stem cell proliferations[3, 4], suggesting the progenitor cells might share similar metabolic patterns with the stem cell during differentiation. Currently, studies are undergoing to understand the key metabolites and underlying biological mechanisms that contribute to these significantly dysregulated metabolic pathways.

S2. *Desulfovibrio alaskensis* G20 Induced Metal Corrosion

Microbially Induced Corrosion (MIC) is a major concern for industrial ferrous metal pipelines and can result in pipeline failure. Sulfate Reducing Bacteria (SRB) have been implicated in contributing to MIC due to their production of corrosive H_2S gas and elemental sulfur along with metal-microbe interactions. This study focuses on the effects of Electron Acceptor Limitation (EAL) and Electron Donor Limitation (EDL) on biofilm physiology and corrosion rate on various surface types, including 1018 carbon steel, 316 stainless steel, and borosilicate glass. *Desulfovibrio alaskensis G20* was grown under steady-state conditions in sulfate-reducing biofilm reactors. Batch cultures grown under EAL and EDL conditions had similar maximum growth rates, but differed significantly in final cell yields at 37°C. Under EAL conditions, biofilms on glass and 1018 steel had elevated biomass levels, both in terms of protein and hexose levels. Under EDL conditions, biofilms on 1018 steel had the highest protein and hexose levels. Differential corrosion rates were observed between EDL and EAL conditions on 1018 carbon steel. The results indicated that different ratios of respiration substrates contributed to altered rates of corrosion, and the difference in corrosion rates could not be explained solely by sulfide, acetate,

or carbohydrate levels. Protecting the 1018 metal coupon from biofilm colonization while maintaining exposure to sulfide was shown to dramatically reduce corrosion.

G20 metabolome extraction and LC-MS based metabolomic profiling.

For the metabolomics analysis, 4-5 replicates of each group of cell samples (electron donor limited and electron acceptor limited G20) were lyophilized then weighed before doing the extraction. The lyophilized cell samples were extracted using a methanol:acetonitrile:water (2:2:1, v/v) solvent mixture. A volume of 1 mL of cold solvent was added to each pellet, vortexed for 30 s and incubated in liquid nitrogen for 1 min. Samples were thawed and sonicated for 10 min. This cycle of cell lysis in liquid nitrogen together with sonication was repeated additional twice times. To precipitate proteins, the samples were incubated for 1 hour at −20 °C, followed by 15 min centrifugation at 13,000 rpm and 4°C. The resulting supernatant was removed and evaporated to dryness in the vacuum concentrator at 10°C. The dry extracts were then reconstituted in acetonitrile:water (1:1, v/v) based on normalization by weights, sonicated for 2 min and centrifuged for 15 min at 13,000 rpm and 4°C to remove insoluble debris. The supernatants were transferred to HPLC vials and stored at −80°C prior to LC-MS analysis.

The LC-MS analysis was performed on an Agilent iFunnel QTOF mass spectrometer (Billerica, MA, USA) linked to an Agilent 1200 series capillary HPLC system (Palo Alto, CA, USA). 8 µL sample was injected after injection volume optimization. A Phenomenex Luna NH2 column (1 mm × 150 mm, 3 µm particle size, 100 Å pore size) was used for LC separation. Mobile phase A was 20 mM ammonium acetate, 40mM ammonium hydroxide in water with 5% acetonitrile, and mobile phase B was acetonitrile with 5% water. The gradient elution profile was as follows: t = 0 min, 100%B; t = 5 min, 100%B; t = 50 min, 0%B; t = 55 min, 0%B; t = 57 min, 100% B; t = 60 min, 100%B. The flow rate was 50 µL/min with 10 min post acquisition time added at 100%B to re-equilibrate the LC column. The m/z scan range was 50−1000, ionization was in negative mode and the scan rate was 2 spectra/sec. All data files were converted to mzXML format and uploaded to XCMS Online to perform a pairwise analysis on non-stressed (n = 5) and $HgCl_2$ stressed (n = 5) using Welch's t-test. For pathway analysis, statistically significant features with fold change > 2.0 and *p*-value < 0.01 were used, resulting in 84 identified pathways, 47 of which had a *p*-value < 0.01.

G20 pathway analysis results.

A total of 12 metabolic pathways were generated using the metabolomic data. Among them, the metabolites L,L-diaminopimelate and (*S*)-2,3,4,5-tetrahydropicolinate were in the lysine biosynthesis pathway were confirmed with MS/MS data from an autonomous workflow. Of particular interest were the lysine biosynthesis and pyrimidine deoxyribonucleotide *de novo* biosynthesis, which are currently under further study (**Supplementary Figure 2**).

S3. *Ercc1*$^{-/\Delta}$ Mouse Model to Study Progeria Syndrome

XPF-ERCC1 endonuclease is required for repair of helix-distorting DNA lesions and cytotoxic DNA interstrand crosslinks[5]. Mild mutations in *XPF* cause the cancer-prone syndrome xeroderma pigmentosum. Mice *Ercc1*$^{-/\Delta}$ have a hypomorphic mutation that is used to model the human XFE progeroid syndrome caused by a mutation in *XPF*, which encodes one subunit of the DNA repair endonuclease XPF-ERCC1. These mice show many aging-related symptoms and a short lifespan. In particular, these mice develop progeroid symptoms in early prepubescence, causing death before sexual maturation and presents an old appearance, weight loss, epidermal atrophy, visual and hearing loss, ataxia, cerebral atrophy, hypertension, liver dysfunction, anemia, osteopenia, kyphosis, sarcopenia and renal insufficiency[5]. Here, we examined the transcriptomic and metabolomic effects caused by a mutation in XPF on the liver tissue of *Ercc1*$^{-/\Delta}$ mouse model by performing global transcriptomic and metabolomic analyses of whole liver tissue samples of seven 12-week old *Ercc1*$^{-/\Delta}$ and seven of their wild-type littermates (C57Bl/6J mice).

The transcriptome dysregulations were monitored using qRT-PCR and 1362 significant gene expression changes were extracted with a fold change > 1.5 and p-value < 0.05. The metabolomic data was generated from HILIC LC-MS analysis on an Agilent iFunnel 6550 in negative mode and processed with XCMS Online using pairwise analysis for wild type (n = 7) and *Ercc1*$^{-/\Delta}$ mice (n = 7). The parameter settings were as follows: centWave for feature detection (Δ m/z = 15 ppm, minimum peak width = 10 s, and maximum peak width = 60 s); obiwarp settings for retention time correction (profStep = 1.0); parameters for chromatogram alignment, including mzwid = 0.015, minfrac = 0.5, and bw = 5. Pathway analysis was performed on statistically significant features (Welch's t-test) with fold change > 1.5 and p-value < 0.01. Transcriptomic and metabolomic data were overlaid using the multi-omic platform in XCMS Online.

The liver was selected as it shows well-defined aging-related changes and DNA repair defects. In our study, a total of 127 dysregulated metabolic pathways were observed with *mummichog*-based analysis of untargeted metabolomic data and 30 of them have evidence of correlating transcriptomic data. Along with the effect of DNA repair defects, we observed several clear metabolic dysregulations on the systems-level (shown in **Supplementary Figure 3**). Remarkably, these systems-level changes due to XPF-ERCC1 deficiency were also associated with normal aging[5].

S4. Human Colon Cancer Study (XCMS Online job ID # 1100254)

Colorectal cancer metabolomic data.

The "one-click" multi-omic approach was applied to an untargeted metabolomic study using patient samples of colon cancer and normal tissues (paired analyses with n=30)[6] (XCMS Online public job ID# 1100254). In brief, metabolites were extracted from tissue samples with organic solvents and analyzed using C18 reverse-phase liquid chromatography (RPLC) coupled to quadrupole time-of-flight mass spectrometry in positive ESI mode. The data was processed in XCMS Online using pairwise analysis and the parameter settings were as follows: centWave for feature detection (Δ m/z = 15 ppm, minimum peak width = 10 s, and maximum peak width = 60 s); obiwarp settings for retention time correction (profStep = 1.0); parameters for chromatogram alignment, including mzwid = 0.015, minfrac = 0.5, and bw = 5. A total of 3908 significant metabolites were discovered with fold change $\geq$ 1.2 and *p*-value $\leq$ 0.05.

Colorectal cancer transcriptomic data.

A comprehensive set of RNAseq transcriptomic data was downloaded from NetGestalt[7]. This data was originally generated from The Cancer Genome Atlas (TCGA) in a study of 22 colon cancer tissue samples vs. 22 normal tissue samples[8]. The gene expression profile was measured using Agilent 244K custom gene expression G4502A-07-3 microarrays and normalized by the LOWESS method. The detailed experimental methods can be found in the supplemental materials of the reference[8]. A total of 10,238 genes with *p*-value $\leq$ 0.01 and fold change $\geq$ 1.2 were selected as dysregulated genes and used for multi-scale omics analysis.

Colorectal cancer proteomic data.

A comprehensive set of shotgun proteomic data was downloaded from netgestalt[7]. The data was originally generated from Clinical Proteomic Tumor Analysis Consortium (CPTAC) in a study of 90 colon cancer tissue samples vs. 30 normal tissue samples[9]. Proteins were extracted from samples and peptides were analyzed on a Thermo LTQ Orbitrap Velos instrument. The detailed experimental methods can be found in the supplemental materials of the reference[9]. A total of 2,545 proteins with *p*-value $\leq$ 0.01 and fold change $\geq$ 1.2 were considered as overexpressed and used for multi-scale omics analysis.

Colorectal cancer multi-omic study results.

In this study, over 7,000 metabolic features were detected; among them over 700 features were statistically significant (*p*-value < 0.01) and used to predict associated metabolic pathways on *mummichog*. These data were originally analyzed by hand over several days to confirm metabolite features, run additional MS/MS experiments to confirm metabolite identity and interpret the pathways.

The automated systems biology platform identified the same significant pathways in a matter of minutes.

Ten metabolic pathways were identified with statistical significance (p-value ≤ 0.01); among them five of the pathways (**Supplementary Figure 4, Supplementary Table 1**) have been previously implicated in the progression of cancer including 1,25-dihydroxyvitamin D3 biosynthesis[10], bile acid biosynthesis[11], zymosterol biosynthesis[12], and ubiquinol-10 biosynthesis[13] and the spermine and spermidine pathway isolated from the original study[6]. Using MS/MS data, we validated three metabolites putatively identified in the predictive pathway analysis, confirming the involvement and upregulation of the spermine and spermidine pathway.

S5. *Desulfovibrio vulgaris* Hildenborough Nitrate Stress

Sulfate reducing bacteria (SRB) have been shown to be useful in heavy-metal bioremediation, yet the presence of nitrate in many contaminated sites result in hindered SRB activity. Previous gene expression and proteomic studies[14] have implicated osmotic stress and nitrite stress response to growth inhibition by upregulation of the glycine/betaine transporter genes and relief of nitrate inhibition of osmoprotectants. Here we look at the model SRB bacterium *Desulfovibrio vulgaris* Hildenborough (DvH) to identify connections between the metabolome of nitrate induced growth inhibition and previous reports to help identify mechanistic response pathways.

DvH cells were prepared in five separate cultures for each non-stressed and $HgCl_2$ stressed sample class. Cultures of DvH were grown up from freezer stocks in 7.5 mL of lactate/sulfate (60 mM/30 mM) medium containing 1% (w/v) yeast extract[15]. The starter cultures were subcultured at OD_{600} of 0.8 after 16 h of growth by transferring 0.5 mL into 10 mL of defined lactate/sulfate medium. Non-stressed subcultures were grown only on defined medium, and nitrate stressed cells were grown on the same medium with the addition of 100 mM sodium nitrate. Non-stressed cells reached mid-late log, OD_{600} of 0.5, after 40 h and were harvested, pelleted and decanted. Pellets were immediately flash frozen in liquid nitrogen and stored on dry ice or at -80˚C. Nitrate stressed cells reached mid-late log after 100 h and were harvested in the same manner.

Metabolomic and Pathway Analysis

Metabolomic analysis was performed in triplicate for each sample on an Agilent 1100 series HPLC coupled to a Bruker Impact II QTOF mass spectrometer (Billerica, MA, USA). A Phenomenex Luna NH2 column (1 mm × 150 mm, 3 µm particle size, 100 Å pore size) was used for LC separation. Mobile phase A was 20 mM ammonium acetate, 40mM ammonium hydroxide in water with 5% acetonitrile, and mobile phase B was acetonitrile with 5% water. The gradient elution profile was as follows: t = 0 min, 100%B; t = 2.5 min, 100%B; t = 50 min, 0%B; t = 55 min, 0%B; t = 57 min, 100%

B; t = 60 min, 100%B. The flow rate was 50 µL/min with 10 min post acquisition time added at 100%B to re-equilibrate the LC column. The m/z scan range was 50−1000, ionization was in negative mode and the scan rate was 2 Hz. All data files were converted to mzXML format and uploaded to XCMS Online to perform a pairwise analysis on non-stressed (n = 5) and $HgCl_2$ stressed (n = 5) using Welch's t-test. For pathway analysis, statistically significant features with fold change > 1.5 and *p*-value < 0.01 were used, resulting in 84 identified pathways, 47 of which had a *p*-value < 0.01.

Multi-omics Analysis

A compilation of gene and protein data from previous studies[14, 16] were used to generate dysregulated lists for comparison with the metabolomic data. In this data set, there was little overlap between highly significant genes and proteins identified in microarray expression and proteomics experiments and the dysregulated metabolic pathways (**Supplementary Figure 5)**. Only *leuA* overlapped with the significantly (*p*-value < 0.01) dysregulated leucine biosynthesis pathway. This may be due to different growth stages of cells at the time harvested and length of nitrate exposure. In this study, cells were grown and stressed with nitrate in the most recent method used to determine gene fitness[17, 18]. The microarray and proteomic data set took cells that were at mid-log and only exposed the cells to nitrate stress for four to eight hours, representing a more immediate response to nitrate stress, but the cultures were unlikely to be actively growing[14, 16]. The cells in this metabolomic data set have 'adapted' to nitrate stress and are actively growing.

Despite the small multi-omics overlap, the pathways that were functioning in a significantly different manner all point to a similar phenomenon. The dysregulation of amino acid biosynthesis and central metabolism cycles can be attributed to nitrate stress via the assimilatory nitrate reduction pathway, which reduces nitrate to ammonium and adds the amine to amino acid precursors. Assimilatory nitrate reduction is not thought to be active in DvH, but these data suggest that it may be functional. The possibility of an active nitrate reductase is further corroborated in the multi-omics data by the increased expression of the second enzyme of the nitrate reduction pathway, nitrite reductase, DVU0625. For pathways with less significant *p*-values, more amino acid biosynthesis was dysregulated corresponding with the above pattern, but also dissimilatory sulfate reduction. The nitrate stressed cells do not grow as well, so we expect to see the sulfate reduction pathway down regulated. If the assimilatory nitrate reduction pathway is inactive, the stress response could also be attributed to energy limitation. Nitrate may compete with sulfate for uptake and transport leaving the cells energy limited. When energy is limiting, cells decrease amino acid biosynthesis and some of the central metabolism pathways. The multi-omics data (dysregulation of leucine biosynthesis, sulfate reduction V, Glycolysis I, and nitrate biosynthesis IV) agree with larger observed responses of DvH to nitrate stress, but pose questions about active metabolic pathways that demand further experimentation.

S6. Bacterial Stress Response Study (XCMS Online job ID # 1133019)

E. coli culture.

To test the efficacy of the multi-omic platform, a standard method for probing changes in metabolomics was developed using *E. coli* K12 MG1655 cultures grown in different carbon sources (glucose and adenosine carbon sources). Glucose and adenosine were prepared with equimolar concentrations of carbon in 10 mL aliquots of M9 minimal media in triplicate. Carbon concentration was based on a final concentration of 20 mM glucose or 0.12 M carbon. All carbon sources were prepared in sterile water, then filtered through a 0.22 µm syringe filter prior to addition to M9 salts. A 10 mL culture of *E. coli* was grown in LB media overnight at 37°C. To inoculate each condition, which was prepared in triplicate, a 1 mL aliquot of cells was centrifuged at 13,000 rpm for 1 minute, the supernatant media was removed and the pellet was washed 3X with sterile water. The cells were made up to a final volume of 1 mL in sterile water and a 1 µL aliquot was added to 8 mL of each carbon source. The cultures were grown until an OD_{600} ~1, or stopped after 72 hours if the growth rate was plateaued. Triplicate 1 mL aliquots were taken for each replicate for metabolomics analysis and duplicate 1 mL samples were taken for RNA sequencing.

E. coli RNA extraction and mRNA-seq.

RNA in *E. coli* samples were extracted using RNeasy Mini Kit (50, Cat. No. 74104) and the extraction procedures followed the protocols inside the extraction kit. In brief, cells were lysed with the working solution and then centrifuged. The supernatants were loaded onto spin column and spun down multiple times to purify RNAs. RNA-seq experiment was performed with 75 bp reads generated on the NextSeq Analyzer located at the Scripps DNA Sequencing Facility. The Genome Analyzer Pipeline Software (currently bcl2fastq/2.16.0.10) is used to perform the early data analysis of a sequencing run, which does the image analysis, base calling, and demultiplexing. Cutadapt software[19] was used to trim the adapter and low base-pair called scores. For mRNA-Seq, STAR 2.3.0 was used to align to genome using the *E. coli* K12 genome reference. EdgeR as used with the method finds number of Differentially Expressed transcripts (DE) significantly changed for the comparisons of different carbon sources. The results are first filtered with False Discovery Rate (FDR) >0.15 and then by *log Counts Per Million* ($\log_2$(CPM)) > 1.0. The $\log_2$ counts-per-million ($\log_2$ CPM) cutoff used to avoid undefined values and the poorly defined log-fold-changes for low counts shrunk towards zero. Further the deviation of the normalized counts within groups can be used to filter out the transcripts with higher variance. We noted that almost all the transcripts were significantly up or down changed.

E. coli metabolome extraction and LC-MS based metabolomic profiling.

For the metabolomics analysis, triplicates of 1 mL of *E. coli* cells (OD_{600} = 1.0) were prepared at each treatment condition (i.e., glucose and adenosine). *E. coli* cells were pelleted by centrifugation at 4°C and 3,200 RCF for 15 min. Subsequently, cell pellets were extracted using a methanol:acetonitrile:water (2:2:1, v/v) solvent mixture. A volume of 1 mL of cold solvent was added to each pellet, vortexed for 30 s and incubated in liquid nitrogen for 1 min. Samples were allowed to thaw and sonicated for 10 min. This cycle of cell lysis in liquid nitrogen together with sonication was repeated additional twice times. To precipitate proteins, the samples were incubated for 1 hour at −20 °C, followed by 15 min centrifugation at 13,000 rpm and 4°C. The resulting supernatant was removed and evaporated to dryness in the SpeedVap at 4°C. The dry extracts were then reconstituted in 100 µL of acetonitrile:water (1:1, v/v), sonicated for 10 min and centrifuged for 15 min at 13,000 rpm and 4°C to remove insoluble debris. The supernatants were transferred to HPLC vials and stored at −80°C prior to LC-MS analysis.

The LC-MS analysis was performed on each sample in triplicate using a Bruker Impact QTOF mass spectrometer (Billerica, MA, USA) linked to an Agilent 1200 series capillary HPLC system (Palo Alto, CA, USA). 2 µL sample was injected after injection volume optimization. A Phenomenex Luna NH2 column (1 mm × 15 cm, 3 µm particle size, 100 Å pore size) was used for LC separation. Mobile phase A was 20 mM ammonium acetate in H_2O with 5% acetonitrile (ACN), and mobile phase B was ACN with 5% H_2O. The gradient elution profile was as follows: t = 0 min, 95%B; t = 5 min, 95%B; t = 50 min, 5%B. t = 63min, 5%B. The flow rate was 50 µL/min. 20 min post acquisition time was also added with 95%B to re-equilibrium the LC column. Injection of 1 µL sodium formate (250 mM) occurred at t = 57 min and eluted on t = 61min. This calibration peak was used to internally calibrate the LC-MS data and also served as the MS peak intensity quality control. The m/z scan range was 25–1500, ionization was in negative mode and acquisition speed was 2 Hz. All data files were converted to mzXML format and uploaded to XCMS Online to perform a pairwise analysis on non-stressed (n = 3) and $HgCl_2$ stressed (n = 3) using Welch's t-test. For pathway analysis, statistically significant features with fold change > 1.5 and *p*-value < 0.01 were used, resulting in 84 identified pathways, 47 of which had a *p*-value < 0.01.

***E. coli* multi-omic analysis result.**

A total of 217 dysregulated metabolic pathways were generated from metabolomic data and 195 (89.9%) of them were putatively confirmed with the analysis of *E. coli* transcriptome. These 195 metabolic pathways show significant changes at both transcriptomic and metabolomic levels. **Supplementary Table 2** lists the system-wide interpretation of 8 top-ranked metabolic pathways. These metabolic pathways were observed to be significantly interrupted and dysregulated after changing the carbon source from glucose to adenosine. As we can see, the most significantly disrupted pathways are

glucose and adenosine related, reflecting the complicated response and molecular regulation of *E. coli* upon the extracellular aberration. In addition, we provided a list of differentially expressed proteins compiled from the studies based on alterations in carbon sources in *E. coli*.[20-23] There is a significant amount of overlap with glycolysis I and II pathways, indicating that our observations are consistent with results from the literature. Most importantly, our systems biology platform provides an opportunity to quickly reveal and understand global molecular changes on a multi-omic level with a convenient "one-click" as demonstrated by both the tabulated results and pathway cloud plot (**Supplementary Figure 6**). We also noticed that there are another 187 metabolic pathways confirmed from the transcriptomic analysis results. These metabolic pathways contain comprehensive details about how *E. coli* response to the change of carbon source and worth further investigation to understand the underlying biology on the systems biology level.

S7. Analysis of 1,600 Serum Samples

The analysis of 1,600 reversed phase LC-MS human plasma serum samples demonstrates the robust capacity of the cloud-based platform. Data was kindly allowed for use from an XCMS user with few experimental details provided. In brief, including pooled quality controls, 1,600 serum samples were analyzed on an Orbitrap-XL MS (Thermo Finnigan – Bremen) coupled to an Accela UHPLC running in positive ionization mode. Chromatographic separation was carried out on a Hypersil-gold C18 column (100 mm x 2.1 mm x 1.9 µm) running a 30 minute gradient from 100% water to 100% methanol. Both mobile phases contained 0.1% formic acid. Raw data files generated were converted in to the mzXML format using the Proteowizard software[24] and up loaded from the University of Manchester onto the XCMS online servers. Data were processed using the centWave algorithm at 3 ppm mass deviation and peak widths ranging from 3–20 s. The obiwarp retention time correction tool using profStep = 1 m/z was also applied alongside the alignment settings of mzwid = 0.015, minfrac = 0.5, and bw = 2. All identifications were detected with a 5 ppm maximum tolerance focusing only on $[M+H]^+$, $[M+Na]^+$, $[M+H-H2O]^+$ and $[M+K]^+$ adducts.

The predictive pathway analysis algorithm provided two highly significant pathways: omega-6 fatty acid metabolism (*p*-value = 0.00093) and mono-unsaturated fatty acid beta-oxidation (*p*-value = 0.00099) (**Supplementary Figure S7**). These pathways are identified by matching high resolution mass spectrometry data to both precursor and adduct ions of the potential metabolites, with more matched features increasing the probability of an accurate pathway match. Additionally, metabolic networking was performed on these putative metabolites, illustrating potential enzymatic activity in one or multiple steps between them.

Supplementary References

1. Li, S.Z. et al. Predicting Network Activity from High Throughput Metabolomics. *PLoS Comput. Biol.* **9**, 11 (2013).
2. Wolswijk, G. Oligodendrocyte precursor cells in the demyelinated multiple sclerosis spinal cord. *Brain* **125**, 338-349 (2002).
3. Panopoulos, A.D. et al. The metabolome of induced pluripotent stem cells reveals metabolic changes occurring in somatic cell reprogramming. *Cell research* **22**, 168-177 (2012).
4. Folmes, C.D. et al. Somatic oxidative bioenergetics transitions into pluripotency-dependent glycolysis to facilitate nuclear reprogramming. *Cell metabolism* **14**, 264-271 (2011).
5. Niedernhofer, L.J. et al. A new progeroid syndrome reveals that genotoxic stress suppresses the somatotroph axis. *Nature* **444**, 1038-1043 (2006).
6. Johnson, C.H. et al. Metabolism links bacterial biofilms and colon carcinogenesis. *Cell metabolism* **21**, 891-897 (2015).
7. Shi, Z., Wang, J. & Zhang, B. NetGestalt: integrating multidimensional omics data over biological networks. *Nature methods* **10**, 597-598 (2013).
8. Muzny, D.M. et al. Comprehensive molecular characterization of human colon and rectal cancer. *Nature* **487**, 330-337 (2012).
9. Zhang, B. et al. Proteogenomic characterization of human colon and rectal cancer. *Nature* **513**, 382-387 (2014).
10. Feldman, D., Krishnan, A.V., Swami, S., Giovannucci, E. & Feldman, B.J. The role of vitamin D in reducing cancer risk and progression. *Nature reviews cancer* **14**, 342-357 (2014).
11. Payne, C.M., Bernstein, C., Dvorak, K. & Bernstein, H. Hydrophobic bile acids, genomic instability, Darwinian selection, and colon carcinogenesis. *Clin Exp Gastroenterol* **1**, 19-47 (2008).
12. Field, A.E. et al. Impact of overweight on the risk of developing common chronic diseases during a 10-year period. *Archives of internal medicine* **161**, 1581-1586 (2001).
13. Frei, B., Kim, M.C. & Ames, B.N. Ubiquinol-10 is an effective lipid-soluble antioxidant at physiological concentrations. *Proceedings of the National Academy of Sciences* **87**, 4879-4883 (1990).
14. He, Q. et al. Impact of elevated nitrate on sulfate-reducing bacteria: a comparative Study of Desulfovibrio vulgaris. *ISME J* **4**, 1386-1397 (2010).
15. Zane, G.M., Yen, H.-c.B. & Wall, J.D. Effect of the Deletion of qmoABC and the Promoter-Distal Gene Encoding a Hypothetical Protein on Sulfate Reduction in Desulfovibrio vulgaris Hildenborough. *Appl. Environ. Microbiol.* **76**, 5500-5509 (2010).
16. Redding, A.M., Mukhopadhyay, A., Joyner, D.C., Hazen, T.C. & Keasling, J.D. Study of nitrate stress in Desulfovibrio vulgaris Hildenborough using iTRAQ proteomics. *Briefings in Functional Genomics & Proteomics* **5**, 133-143 (2006).
17. Korte, H.L. et al. Independence of Nitrate and Nitrite Inhibition of Desulfovibrio vulgaris Hildenborough and Use of Nitrite as a Substrate for Growth. *Environmental Science & Technology* **49**, 924-931 (2015).
18. Korte, H.L. et al. Genetic basis for nitrate resistance in Desulfovibrio strains. *Frontiers in Microbiology* **5** (2014).
19. Martin, M. Cutadapt removes adapter sequences from high-throughput sequencing reads. *2011* **17** (2011).
20. Du, Z., Nandakumar, R., Nickerson, K.W. & Li, X. Proteomic adaptations to starvation prepare Escherichia coli for disinfection tolerance. *Water Res.* **69**, 110-119 (2015).
21. Vijayendran, C., Burgemeister, S., Friehs, K., Niehaus, K. & Flaschel, E. 2DBase: 2D-PAGE database of Escherichia coli. *Biochemical and Biophysical Research Communications* **363**, 822-827 (2007).
22. Vijayendran, C. et al. The plasticity of global proteome and genome expression analyzed in closely related W3110 and MG1655 strains of a well-studied model organism, Escherichia coli-K12. *J. Biotechnol.* **128**, 747-761 (2007).
23. McKee, A.E. et al. Manipulation of the carbon storage regulator system for metabolite remodeling and biofuel production in Escherichia coli. *Microb. Cell. Fact.* **11**, 12 (2012).
24. Chambers, M.C. et al. A cross-platform toolkit for mass spectrometry and proteomics. *Nature biotechnology* **30**, 918-920 (2012).

Supplementary Tables

Supplementary Table 1. Colon cancer pathway analysis

	Metabolic Pathway	Metabolites	Biological significance
1	Spermine and spermidine degradation	N^1-acetylspermine, N^1-acetylspermidine, spermidine	Polyamines are associated with increased cellular proliferation in colon cancer tissues[6]
2	1,25-dihydroxyvitamin D_3 biosynthesis	1,25-dihydroxy vitamin D_3	Vitamin D_3 deficiency leads to cancer development[10]
3	Bile acid biosynthesis	Bile acids	Bile acid interact with epithelial cells causing mutations that lead to cancer
4	Zymosterol biosynthesis	Zymosterol	Increased cholesterol arising from zymosterol metabolism is correlated with colon cancer[23, 24]
5	Ubiquinol-10 biosynthesis	Ubiquinol-10	Ubiquinol-10 is an antioxidant that can prevent cancer[13]

Supplementary Table 2. *E. coli* K12 MG1655 multi-omics analysis.

Pathway	Dysreg. gene	Tot. gene	Dysreg. prot.	Tot. prot.	Dysreg. metab.	Tot. metab.	*p*-value
Pyrimidine deoxyribonucleoside *de novo* biosynthesis I	3	7	0	7	12	15	0.012
Glycolysis I	12	18	7	18	11	14	0.016
Glycolysis II	11	18	6	18	11	14	0.016
Puring deoxyribonucleoside degradation I	2	2	0	2	7	8	0.020
UDP-*N*-acetyl-D-glucosamine biosynthesis I	2	4	1	4	8	10	0.027
Galactose degradation I	1	5	0	5	8	10	0.027
4-aminobutanoate degradation I	1	2	0	2	6	7	0.034
Pyrimidine deoxyribo-nucleosides degradation	1	2	0	2	6	7	0.034